PNAS RESEARCH ARTICLE | IMMUNOLOGY AND INFLAMMATION OPEN ACCESS

Single-cell analysis of refractory anti-SRP necrotizing myopathy treated with anti-BCMA CAR-T cell therapy

Chuan Qin[a,b,1], Ming-Hao Dong[a,b,1], Luo-Qi Zhou[a,b], Wen Wang[c], Song-Bai Cai[c], Yun-Fan You[a,b], Ke Shang[a,b], Jun Xiao[a,b], Di Wang[d], Chun-Rui Li[d], Min Zhang[a,b], Bi-Tao Bu[a,b,2], Dai-Shi Tian[a,b,2], and Wei Wang[a,b,2]

Edited by Lawrence Steinman, Stanford University, Stanford, CA; received September 19, 2023; accepted December 26, 2023

Immune-mediated necrotizing myopathy (IMNM) is an autoimmune disorder associated with the presence of autoantibodies, characterized by severe clinical presentation with rapidly progressive muscular weakness and elevated levels of creatine kinase, while traditional pharmacological approaches possess varying and often limited effects. Considering the pathogenic role of autoantibodies, chimeric antigen receptor (CAR)-T cells targeting B cell maturation antigen (BCMA) have emerged as a promising therapeutic strategy. We reported here a patient with anti-signal recognition particle IMNM refractory to multiple available therapies, who was treated with BCMA-targeting CAR-T cells, exhibited favorable safety profiles, sustained reduction in pathogenic autoantibodies, and persistent clinical improvements over 18 mo. Longitudinal single-cell RNA, B cell receptor, T cell receptor sequencing analysis presented the normalization of immune microenvironment after CAR-T cell infusion, including reconstitution of B cell lineages, replacement of T cell subclusters, and suppression of overactivated immune cells. Analysis on characteristics of CAR-T cells in IMNM demonstrated a more active expansion of $CD8^+$ CAR-T cells, with a dynamic phenotype shifting pattern similar in $CD4^+$ and $CD8^+$ CAR-T cells. A comparison of $CD8^+$ CAR-T cells in patients with IMNM and those with malignancies collected at different timepoints revealed a more NK-like phenotype with enhanced tendency of cell death and neuroinflammation and inhibited proliferating ability of $CD8^+$ CAR-T cells in IMNM while neuroinflammation might be the distinct characteristics. Further studies are warranted to define the molecular features of CAR-T cells in autoimmunity and to seek higher efficiency and longer persistence of CAR-T cells in treating autoimmune disorders.

chimeric antigen receptor (CAR) T cell | immune mediated necrotizing myopathy | B cell maturation antigen | single-cell RNA sequencing

Significance

The present study illustrates great potentials of chimeric antigen receptor (CAR-T) cells targeting B cell maturation antigen in treating anti-signal recognition particle myopathy, with sustained depletion of autoantibodies and therapeutic efficacies beyond 18 mo. Moreover, by comparing single-cell profiles of CAR-T cells from patients with IMNM and those from patients with malignancies, our data show the distinct characteristics of CAR-T cells in human with autoimmunity, which may guide future improvement of CAR-T therapy in autoimmune diseases.

Immune-mediated necrotizing myopathy (IMNM) is a distinct and common form of inflammatory myopathy, characterized by symmetrical muscle weakness, exceptionally high creatine kinase (CK) levels, and muscle necrosis or regeneration (1, 2). IMNM was newly identified as a separate entity in 2004, with increasing recognition of its challenges to treat. Autoantibodies recognizing signal recognition particle (SRP) have been described in association with IMNM. Of note, despite intense immunotherapy, refractory or relapsed disease has been reported in a significant subset of anti-SRP myopathy. Additionally, younger patients tend to have poorer neurological recovery (3, 4).

B cell maturation antigen (BCMA), primarily expressed by plasmablasts and plasma cells, could serve as a potential target for antibody-associated autoimmune disorders. Chimeric antigen receptor (CAR) T cell therapy has recently extended to autoimmune diseases (5). Given the pathogenic role of SRP-IgG, CAR-BCMA T cell therapy might have therapeutic potentials in treating refractory anti-SRP myopathy.

Here, we report a case of highly refractory anti-SRP myopathy who received treatment with anti-BCMA CAR-T cells and showed prolonged remission beyond 18 mo. To gain further insights into the immune microenvironment changes following CAR-T therapy and the characteristics of CAR-T cells in patients with IMNM, we conducted single-cell RNA-sequencing (scRNA-seq), T cell receptor-sequencing (TCR-seq), and B cell receptor-sequencing (BCR-seq) analysis on samples collected before and after infusion, as well as the matching CAR-T infusion product. Besides clearance of B cell lineage after CAR-T therapy, we observed suppressed humoral immune response and inflammatory response of the immune microenvironment. By longitudinal CAR-T cells proportion analysis and clone tracking, we observed a significant expansion of $CD8^+$ CAR-T cells and a similar shifting pattern in $CD4^+$ and $CD8^+$ CAR-T cells. Furthermore, we found that $CD8^+$ CAR-T cells collected at 1 mo post-infusion in IMNM were more likely to function at a remission/stable stage, but presented compromised proliferation properties and enhanced features of NK-cell signaling and cell death when compared to CAR-T cells

Author contributions: C.Q., Wen Wang, D.W., C.-R.L., M.Z., B.-T.B., D.-S.T., and Wei Wang designed research; C.Q., M.-H.D., L.-Q.Z., Y.-F.Y., K.S., J.X., D.W., C.-R.L., M.Z., B.-T.B., D.-S.T., and Wei Wang performed research; C.Q., M.-H.D., L.-Q.Z., Y.-F.Y., C.-R.L., D.-S.T., and Wei Wang analyzed data; and C.Q., M.-H.D., Wen Wang, S.-B.C., K.S., J.X., B.-T.B., D.-S.T., and Wei Wang wrote the paper.

Competing interest statement: Wen Wang and S.-B.C. are employees of Nanjing IASO Therapeutics Ltd. and held interests in the company. Wen Wang held interests in patent applications related to the CT103A. All other authors declare no competing interest.

This article is a PNAS Direct Submission.

[1]C.Q. and M.-H.D. contributed equally to this work.

[2]To whom correspondence may be addressed. Email: bubitao@tjh.tjmu.edu.cn, tiands@tjh.tjmu.edu.cn, or wwang@tjh.tjmu.edu.cn.

This article contains supporting information online at https://www.pnas.org/lookup/suppl/doi:10.1073/pnas.2315990121/-/DCSupplemental.

Published January 30, 2024.

manufactured from patients with malignancies. Moreover, neuroinflammation was suggested to be the distinctive signature of $CD8^+$ CAR-T cells in IMNM.

Methods

Human Subjects and Treatment Procedure. This study was approved by the Institutional Review Board of Tongji Hospital (TJ-IRB20220101). Written informed consent for the use of the CAR-T infusion product and blood samples and disclosure of deidentified health information in research were obtained. The anti-BCMA CAR-T cells, CT103A, were manufactured by IASO Biotherapeutics, which have been described and used in our previous studies in multiple myeloma patients (6) and NMOSD patients (7). To enhance the expansion and engraftment of the transferred cells, a lymphodepletion regimen was administered prior to CAR-T cell infusion (8). Before lymphodepletion therapy, the participant discontinued all maintenance therapy, including immunosuppressants and steroids, for 1 to 3 d before treatment initiation. Then, the participant received a lymphodepletion therapy with an FC regimen consisting of cyclophosphamide 500 mg/m^2 plus fludarabine 30 mg/m^2 (on −4, −3, −2 d before infusion), and a single dose of 1.0×10^6 total CAR-T cells per kilogram body-weight (±20%) on day 0. Results were reported here to a data cut-off of September 12, 2023, with follow-up beyond 18 mo. Detailed materials and methods are available in *SI Appendix*.

Results

Patients' Characteristics and Clinical Response. The patient was a 25-y-old man, who had a 7-y history of anti-SRP antibody seropositive IMNM (1) and concomitantly suffered from Sjögren's syndrome (SS). At disease onset, he presented with weakness in the proximal limbs and markedly elevated serum CK levels over 16,000 U/L, but without extramuscular involvement. The diagnosis of IMNM was confirmed by anti-SRP-IgG detection and muscle biopsy showing active fiber necrosis mixed with regeneration and mild inflammation (3). The patient received multiple immunomodulatory therapies (Fig. 1*A*), including pulsed/oral steroids, tacrolimus, methotrexate, rituximab, tocilizumab, mycophenolate mofetil, cyclosporin A, cyclophosphamide, plasma exchange, regular intravenous immune globulin (IVIg), and mesenchymal stem cell infusion (once, 8 mo before enrollment), but still suffered from persistent impairments with recurrent attacks. At the time of enrollment, he was paralyzed and bed-ridden, with the inability to lift his arms above his head [grade 4- Medical Research Council (MRC) score] or get up from the bed without assistance (grade 2- MRC score) and elevated CK levels of 4,806 IU/L, exhibiting severe signs of clinical and radiographic progression, even under regular administration of IVIg (2.0 g/kg, every 4 wk), oral prednisone (25 mg/d), tocilizumab (8 mg/kg, 480 mg in total, every 4 wk), and methotrexate (15 mg/wk) (Fig. 1*A*).

Anti-BCMA CAR-T therapy was discussed and performed with the patient's written consent. All immunomodulatory treatments including steroid were discontinued before lymphodepletion therapy. Cyclophosphamide plus fludarabine was given for 3 consecutive days, and $6.534*10^7$ anti-BCMA CAR-T cells (CT103A, $0.93*10^6$ cell/kg body weight) with transfection efficacy of 48% were administered on March 7, 2022 (Fig. 1*B*). CAR-T cells rapidly expanded, peaked at 10 d, and then gradually declined within 2 mo (Fig. 1 *C* and *D*). Following CAR-BCMA T cells infusion, the patient experienced transient grade 1 CRS (fever to 39.2 °C) and was treated with 40 mg methylprednisolone once at day 9. Transient cytopenia and cytokine release were observed but resolved within 2 mo (Fig. 1*E*). By the third month, he showed improvements in upper limb strength (no limitations to lift his arms) and lower limb strength with the regained ability to walk. At the 9-mo follow-up, he exhibited a near-normal neurological examination, with only a mild residual weakness (grade 4 MRC score) in proximal lower extremity muscles, and normal strength (grade 5 MRC score) in the neck, distal lower extremity, and all upper extremity muscles. He was able to get up from the floor and walk without assistance (Manual Muscle Testing-8 score from 96 at baseline to 137 at the last visit, Fig. 1*F*). The levels of serum CK declined from 4,778 before treatment to 260 IU/L after 18 mo, and myoglobin level decreased from 837 to 66.2 ng/mL (Fig. 1*G*). Arm and thigh MRI at the 18-mo follow-up demonstrated reduced active muscle lesions of enhanced T1 signal (Fig. 1*H*). The clinical and radiographic improvement have persisted up to the data cut-off of September 12, 2023 (over 18 mo), without any additional immunomodulatory treatments or steroid administration.

$CD3^-$ $CD19^+$ total B cells were undetectable within the first 2 mo, while $CD4^+$ T cells, $CD8^+$ T cells, and natural killer cells being fluctuated (Fig. 1 *I*–*K*), possibly due to lymphodepletion therapy and CAR-T cells expansion. Notably, circulating B cells gradually returned to normal ranges, with approximately 90% of the reconstituted B cells being $CD19^+$ $CD27^-$ IgD^+ naive B cells, and a low presence of $CD27^+$ IgD^- switched memory B cells (Fig. 1*K*). A significant decrease in total IgG after CAR-T cell infusion was observed (Fig. 1*L*), however, with no need for long-term or regular intravenous immunoglobulin replacement. The levels of both anti-SRP and anti-Ro52 autoantibodies in serum declined and remained negative beyond 18 mo (Fig. 1*M*). As for the concomitant SS, the decrease in pathogenic autoantibodies (anti-SSA-IgG) and the increase in tear film breakup time (5 s to 14 s in the right eye, and 3 s to 10 s in the left eye) were observed from baseline to the last visit, suggesting both serologic remission and clinical improvement related to SS.

Immune Alterations Following CAR-T Therapy. To illustrate the altered cellular profiles during CAR-T therapy, we performed longitudinal 5′ single-cell RNA-sequencing (scRNA-seq), T cell receptor-sequencing (TCR-seq), and B cell receptor-sequencing (BCR-seq) on peripheral blood mononuclear cells from the IMNM patient at baseline, 1 mo, 3 mo, 6 mo, 9 mo, 12 mo, 15 mo, and 18 mo after infusion. A total of 68,350 high-quality cells were profiled, with 27,108 paired TCR sequences out of 32,566 T cells (83%) and 4,981 paired BCR sequences out of 5,670 B cells (88%; Fig. 2*A*). By clustering and annotation, we identified 15 diverse immune cell types based on canonical markers (Fig. 2*B*). Subsequent cell-density analysis and cell-type counting showed relatively obvious differences in cellular composition pre- and post-infusion. In accordance with the results of flow cytometry (Fig. 1*K*), B cell lineage showed a noticeable decrease at 1 mo, followed by a step-by-step recovery post-infusion, primarily consisting of $CD19^+$ $CD27^-$ IgD^+ B naive cells. Additionally, we observed a significant expansion of $CD8^+$ Te cells and remarkable reduction in $CD4^+$ T cells post-infusion, suggesting the suppressed proliferation of autoreactive $CD4^+$ T cells triggered by clonally expanded $CD8^+$ T cells in autoimmune diseases as previously reported (9, 10). Perhaps due to lymphodepletion therapy, the proportion of myeloid cells raised at 1 mo and descended to the baseline level post-infusion (Fig. 2 *C* and *D*). Despite the changes in cellular composition, ssGSEA analysis demonstrated that CAR-T therapy led to suppressed immune responses and inflammation-related signatures of endogenous T cells, NK cells, and myeloid cells (Fig. 2*E*), indicating that CAR-T therapy might also contribute to the improvement of immune microenvironment except for reconstitution of B cell lineages.

Re-clustering of B cells and plasma cells identified six clusters that were annotated based on canonical marker expression,

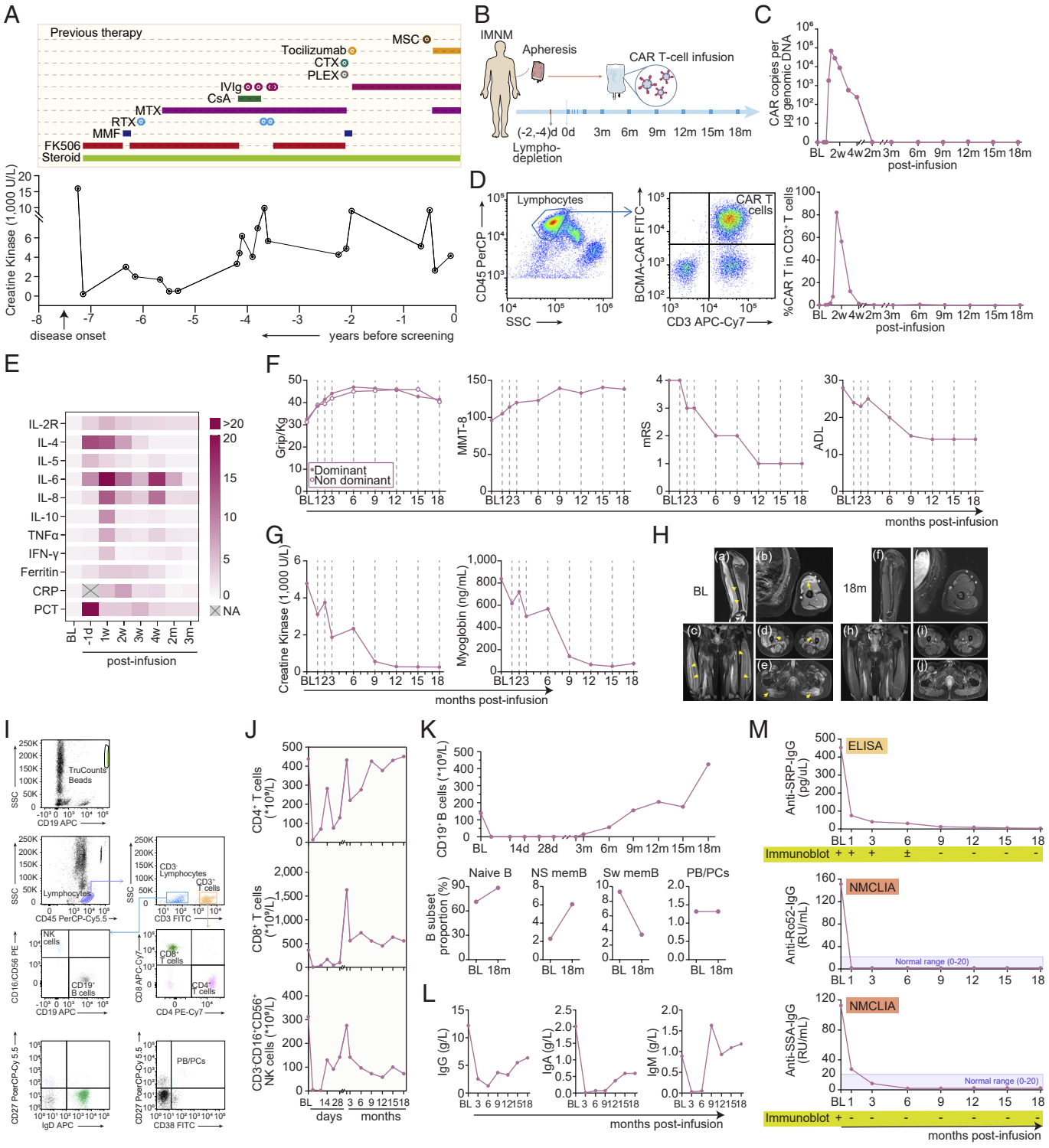

Fig. 1. Clinical evaluation following CAR-T cell infusion. (*A*) Serum creatine kinase (CK) levels before screening, with previous immunosuppressive therapies. (*B*) A schematic overview of treatment procedure. (*C*) Kinetics of CAR copies per μg genomic DNA detected by droplet digital PCR. (*D*) Representative images and kinetic changes of CAR-T cells percentage in $CD3^+$ T cells detected by flowcytometry. (*E*) Heatmap showing kinetic changes of inflammatory factors in blood following CAR-T cell infusion. Interleukin, IL; tumor necrosis factor, TNF; interferon, IFN; CRP, C-reactive protein; PCT, procalcitonin. Average levels are normalized from baseline. (*F*) Kinetic parameters measuring clinical response following CAR-T cell infusion, including the grip strength, the MMT-8 (with a maximum score of 150 when tested bilaterally without presentation of muscle weakness), modified Rankin Score (mRS) score (range 0 to 6, from health without symptoms to death), and activities of daily living (ADL) scale score (14-item, range 14 to 56, from maximal independence to maximal disability). (*G*) Kinetic levels of creatine kinase and myoglobin levels in serum. (*H*) Representative Gadolinium-enhanced T1-weighted (Gd-T1w) MR images showing abnormally enhanced signal (active lesions, arrows) in the left biceps (*a* and *b*), vastus lateralis (*c*), vastus intermedius (*d*), and gluteus maximus (*e*), at baseline (*a*–*e*) and at 18 mo post-infusion (*f*–*j*). (*I* and *J*) Representative plots of flowcytometry and kinetic changes of $CD4^+$ T cells, $CD8^+$ T cells, and $CD3^-$ $CD16^+$ NK cells levels in blood at indicated time points post-infusion. (*K*) Kinetic changes of circulating $CD19^+$ B cells, and the proportion of $CD19^+$ $CD27^-$ IgD^+ naive B cells, $CD19^+$ $CD27^+$ IgD^+ non-switched memory B cells (NS mem), $CD19^+$ $CD27^+$ IgD^- switched memory B cells (Sw mem), and $CD27^+$ $CD38^+$ plasmablasts and plasma cells (PB/PCs) in total B cells. (*L*) Kinetic changes of IgG, IgA, and IgM in blood pre- and post-infusion. (*M*) Kinetic changes of anti-SRP-IgG, anti-Ro52-IgG, and anti-SSA-IgG levels were detected by enzyme-linked immunosorbent assay (ELISA), magnetic nanoparticle chemiluminescence immunoassay (NMCLIA), and immunoblots.

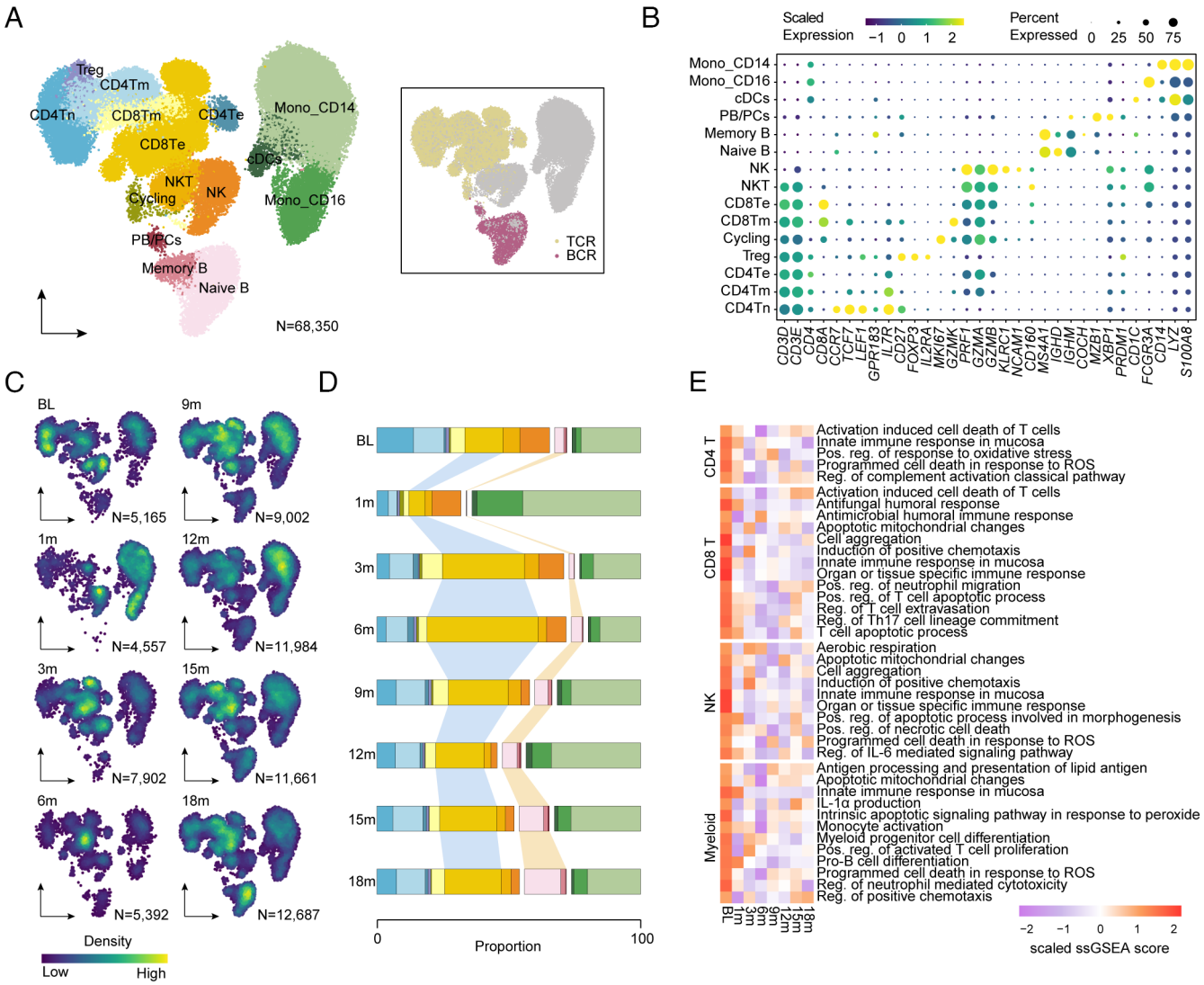

Fig. 2. Immune alterations following CAR-T cell therapy. (*A*) Uniform manifold approximation and projection (UMAP) plot of 68,350 single-cell transcriptomes of peripheral blood mononuclear cells integrated from the patient with IMNM at baseline, at 1 mo, at 3 mo, at 6 mo, at 9 mo, at 12 mo, at 15 mo, and at 18 mo post-infusion. Clusters denoted by color are labeled with inferred cell types, including four CD4$^+$ T cell clusters, two CD8$^+$ T cell clusters, cycling cells (Cycling), NK cells, NKT cells, two monocyte clusters, conventional dendritic cells (cDCs), and three B cell clusters. UMAP of cells colored by BCR and TCR detection. (*B*) Dot plot showing cell clusters denoted by gene expression of known markers. (*C*) UMAP plots showing cell density of peripheral blood mononuclear cell (PBMC) cells integrated from the patient with IMNM at baseline, at 1 mo, at 3 mo, at 6 mo, at 9 mo, at 12 mo, at 15 mo, and at 18 mo post-infusion. (*D*) Bar plots of the proportion of cell types in PBMC cells integrated from the patient with IMNM at baseline, at 1 mo, at 3 mo, at 6 mo, at 9 mo, at 12 mo, at 15 mo, and at 18 mo post-infusion. (*E*) Heatmap showing single-sample gene set enrichment analysis (GSEA) scores of indicated signatures in CD4$^+$ T cells, CD8$^+$ T cells, NK cells, and myeloid cells of patient with IMNM at baseline, at 1 mo, at 3 mo, at 6 mo, at 9 mo, at 12 mo, at 15 mo, and at 18 mo post-infusion.

including immature, naive, non-switched and switched memory, double-negative B cells and PB/PCs (Fig. 3 *A*–*C* and *SI Appendix*, Fig. S1*A*). PB/PCs, which were deemed as the main BCMA-expressed cells responsible for producing pathogenic antibodies, were successfully eliminated at 1 mo post BCMA-targeted CAR-T therapy (Fig. 3*C* and *SI Appendix*, Fig. S1*B*). B cell lineage was gradually restored after 3 mo post-infusion and we observed a significantly lower clonality and higher diversity of restored B cells compared with those at baseline (Fig. 3*D*). Furthermore, we conducted the sequence alignment analysis to compare the CDRH3 sequences of B cells at different time-points and there was no overlap between B cells at baseline and B cells collected at any other time-point (Fig. 3*E* and *SI Appendix*, Fig. S1*C*), suggestive of the efficient removal of abnormal pathogenic B cell lineage and successful generation of brand-new B cells with distinct clone types. Moreover, 1,366 differentially expressed genes were identified when comparing B cells at baseline with restored B cells at 18 mo post-infusion (P-value < 0.05, $\log_2$FoldChange > 0.2) (Fig. 3*F*) and subsequent functional enrichment analysis demonstrated markedly down-regulated pathways and lower expression of genes related with B cell function and energy metabolism in restored B cells (Fig. 3 *G* and *H*), suggesting that B cells were normalized from an overactivated status to a close-to-natural condition that could produce a certain level of defensive antibodies rather than pathogenetic antibodies after CAR-T therapy (Fig. 1 *L* and *M*).

We subsequently conducted a detailed analysis of endogenous T cells by fine-resolution re-clustering and identified 11 final clusters with canonical marker expression (Fig. 4 *A* and *B*). Notably, CD8$^+$ Te cells were further subdivided into three more refined clusters, termed CD8$^+$ Te-1/2/3, and all three clusters exhibited a significant increase in proportion at 3 mo after CAR-T therapy and remained relatively stable during the subsequent follow-up (Fig. 4*C*). Paired T cell receptor analysis revealed a significant

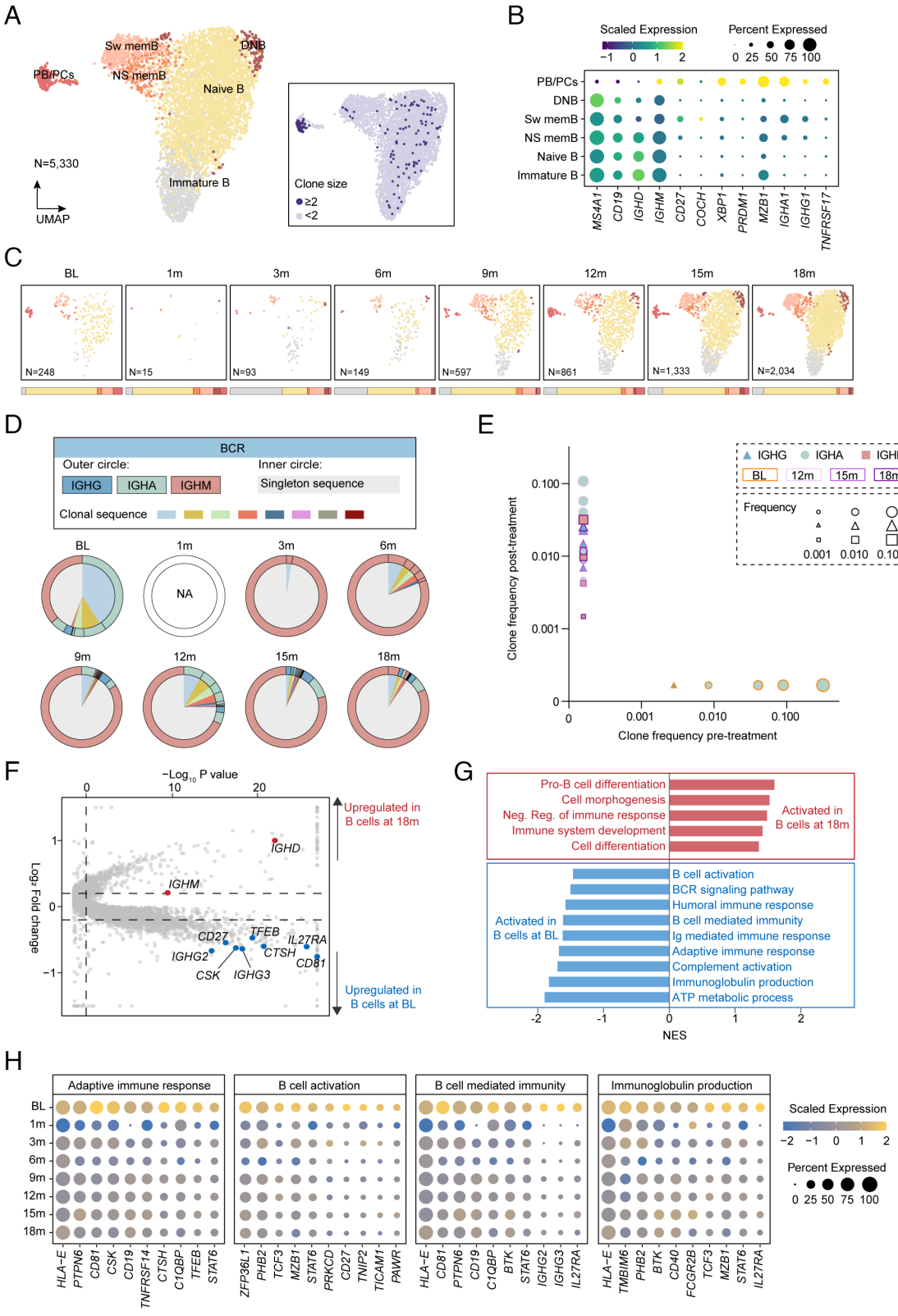

Fig. 3. Compositional and clonal analysis of B lymphocytes following CAR-T cell therapy. (*A*) UMAP plots showing re-clustering of B cells colored by six subsets, annotated as immature, naive, non-switched memory (NS mem), switched memory (Sw mem), double negative (DN) B cells, and plasmablasts and plasma cells (PB/PCs). UMAP plot of B cell subsets colored by clone size (number of cells belonging to a specific clone type), showing significant clonal expansion. (*B*) Dot plot showing cell clusters denoted by gene expression of known markers. (*C*) UMAP plots showing cell distribution of B cells integrated from the patient with IMNM at baseline, at 1 mo, at 3 mo, at 6 mo, at 9 mo, at 12 mo, at 15 mo, and at 18 mo post-infusion. (*D*) Individual repertories from B cells integrated from the patient with IMNM at baseline, at 1 mo, at 3 mo, at 6 mo, at 9 mo, at 12 mo, at 15 mo, and at 18 mo post-infusion. For the inner circle, colored wedges represent expanded clones and gray area represents singleton sequence. For the outer circle, colored edges represent immunoglobulin classes. (*E*) Scatterplot comparing BCR clone frequencies between B cells integrated from the patient with IMNM at baseline and at 12 mo/15 mo/18 mo, respectively. (*F*) Volcano plot showing differential expression analysis comparing B cells integrated from the patient with IMNM at baseline to those at 18 mo post-infusion. (*G*) GSEA analysis showing significantly changed pathways comparing B cells integrated from the patient with IMNM at baseline to those at 18 mo post-infusion. (*H*) Dot plots of genes related to adaptive immune response, B cell activation, B cell-mediated immunity, and Ig production of B cells integrated from the patient with IMNM at baseline, at 1 mo, at 3 mo, at 6 mo, at 9 mo, at 12 mo, at 15 mo, and at 18 mo post-infusion.

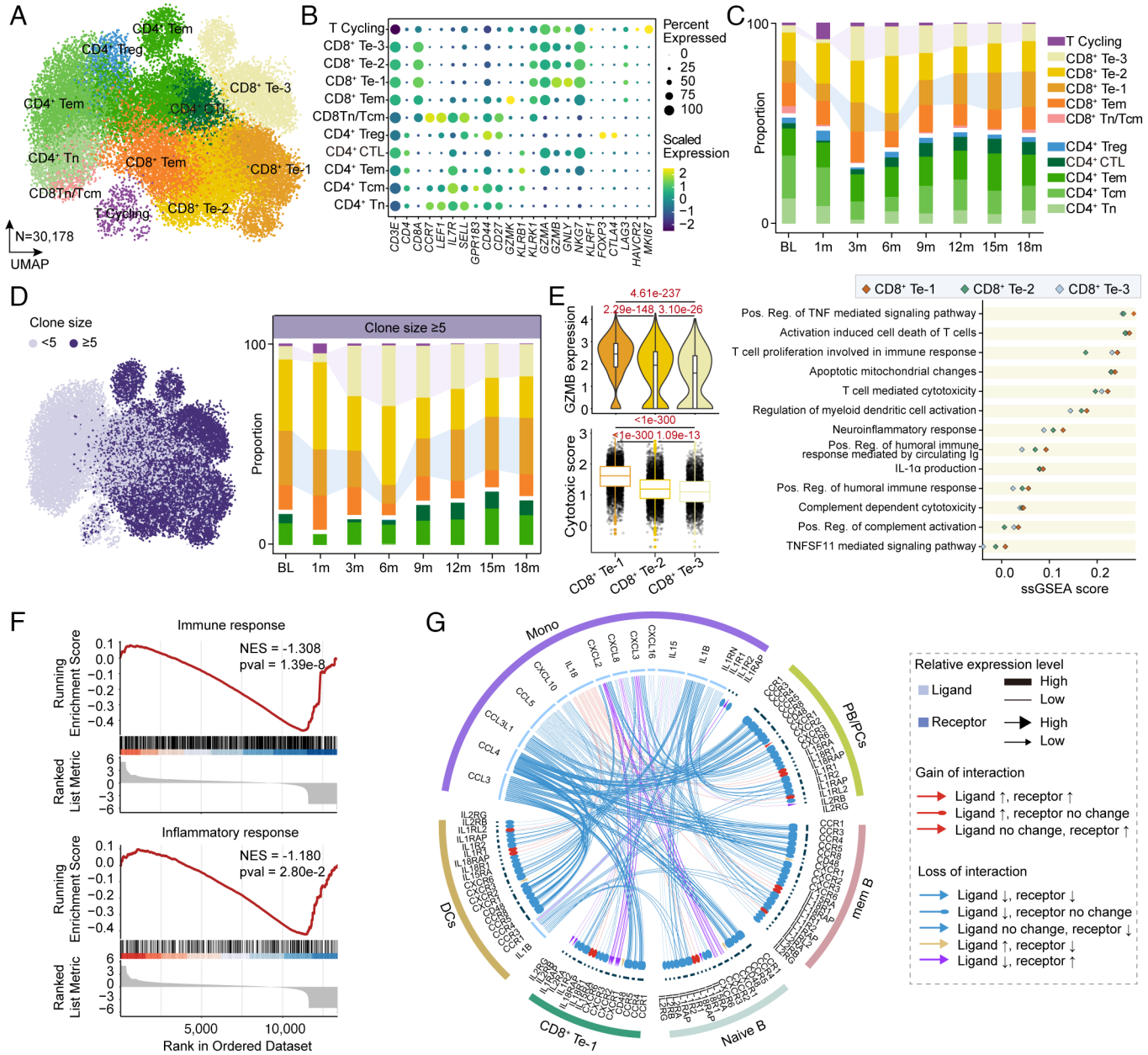

Fig. 4. Compositional and clonal analysis of endogenous T lymphocytes following CAR-T cell therapy. (*A*) UMAP plots showing re-clustering of T cells colored by 11 subsets, including five CD4$^+$ T cell clusters, five CD8$^+$ T cell clusters, and cycling T cells (T Cycling). (*B*) Dot plot showing cell clusters denoted by gene expression of known markers. (*C*) Bar plots of the proportion of cell types in re-clustered T cells integrated from the patient with IMNM at baseline, at 1 mo, at 3 mo, at 6 mo, at 9 mo, at 12 mo, at 15 mo, and at 18 mo post-infusion. (*D*) UMAP plot of T cell subsets colored by clone size, showing significant clonal expansion. Bar plots showing the frequency of clonal T cells. ≥5 clones denote clonotypes observed more than fourth time. (*E*) Violin plots showing *GZMB* (granzyme B) expression and Box plots showing signature enrichment of Cytotoxic in cells of three CD8$^+$ Te clusters. Boxes show median, Q1 and Q3 quartiles and whiskers up to 1.5× interquartile range. Pairwise comparisons were performed using a two-sided Wilcoxon rank-sum test with a Benjamini–Hochberg correction. Scatter plot showing single-sample GSEA scores of indicated signatures (upregulated in CD8$^+$ Te-1 cells) in cells of three CD8$^+$ Te clusters. (*F*) GSEA analysis showed inhibited enrichment of immune response and inflammatory response in re-clustered T cells integrated from the patient with IMNM at 18 mo compared with those at baseline. (*G*) Circos plots showing gained/lost cytokine-related cell–cell communication at 18 mo post-infusion compared to baseline between CD8$^+$ Te-1 cells and other cell types.

expansion of highly frequent clonotypes (clonotype frequency ≥5) in CD8$^+$ Te-3 cells across the clinical visit while highly expanded CD8$^+$ Te-1 cells showed a certain degree of decrease at 3 mo and at 6 mo post-infusion, followed by a gradual restoration (Fig. 4*D*). Further exploration of differential gene expression identification, gene module scoring, and GSVA analysis indicated that CD8$^+$ Te-3 cells, characterized by relatively lower expression of *GZMB* (granzyme B) and higher expression of *CCL5* (C-C motif chemokine ligand 5), and *KLRG1* (killer cell lectin–like receptor G1), presented a signature of enhanced cell chemotaxis and NK receptor (Fig. 4*E* and *SI Appendix*, Fig. S2 *A* and *B*), which might assist to eliminate pathogenic cells and promote cell survival, as NK receptors could provide needed signals to avoid activation-induced cell death induced by TCR as previously reported (11). In contrast, CD8$^+$ Te-1 cells with higher *GZMB* expression exerted a more cytotoxic and neuroinflammation signature and were inclined to facilitate humoral immune responses (Fig. 4*E*). Moreover, restored CD8$^+$ Te-1 cells at 18 mo post-infusion presented an attenuated feature of immune response and inflammatory response (Fig. 4*F* and *SI Appendix*, Fig. S2*C*) and shared obviously reduced cytokine-related interactions with other cell types (Fig. 4*G*) when compared with those at baseline, suggesting that the excessive

immune and inflammatory effect of CD8$^+$ Te-1 cells could be also partially normalized after CAR-T therapy.

CAR-T Cell Characteristics after Infusion in Patients with IMNM. To investigate how transferred CAR-T cells might function in vivo and be shaped by the host immunological milieu, we further conducted scRNA-seq and paired TCR-seq on infusion product (IP) of this IMNM patient as well as CAR-T cells in vivo at 1 mo after infusion sorted by flow cytometry. By integrating and re-clustering T cells collected at baseline, IP, CAR-T cells, and endogenous T cells at 1 mo, distinct T cells clusters were identified: CCR7$^+$ LEF1$^+$ naive T cells (Tn), CCR7$^+$ GPR183$^+$ central memory T cells (Tcm), CCR7$^-$ GPR183$^+$ GZMK$^+$ effector memory T cells (Tem), CD8$^+$ GZMB$^+$ NKG7$^+$ effector T cells (Te), CD4$^+$ NKG7$^+$ cytotoxic T cells (CD4$^+$ CTLs), and CD4$^+$ FOXP3$^+$ regulatory T cells (CD4$^+$ Treg) using canonical markers (Fig. 5 *A* and *B*). Furthermore, it was found that the cycling effector phenotype (cycling Te, MKI67$^+$ GZMB^{lo}) was the most prevalent cell type in IPs, with a balanced proportion of CD4$^+$ and CD8$^+$ cells, likely due to stimulation during manufacturing. In the IP, CD4$^+$ CAR-T cells possessed a higher proportion, but this dominance diminished in CAR-T cells at 1 mo post-infusion (Fig. 5*C*), suggestive of a more significant expansion and a more pivotal effect of CD8$^+$ CAR-T cells. Subsequent clone tracking analysis demonstrated that dominant CD8$^+$ TCR clones within 1 mo in vivo primarily originated from endogenous Te and Tem cells at baseline, then manufactured into cycling effector phenotype in IP, and differentiated into Te cells after infusion (Fig. 5*D*). CD4$^+$ CAR-T cells presented a similar dynamic pattern (Fig. 5*D*) but tended to maintain an effector memory manner at 1 mo (Fig. 5*C*). Consistent with phenotype changes in CAR-T cells, gene module scoring indicated distinct effector signature and impaired proliferation and energy metabolism features in CD4$^+$ and CD8$^+$ CAR-T cells at 1 mo in vivo (Fig. 5*E*).

We next aimed to identify the unique characteristics of CD8$^+$ CAR-T cells in vivo originated from IMNM patient, which are often considered as the primary effector of CAR-T therapy. To that end, we integrated our transcriptome profiles of sorted CAR-T cells collected at 1 mo in vivo with four external published datasets (GSE151310, GSE197268, GSE166352, and GSE125881), including 1) CAR-BCMA T cells collected at peak phase (day 8) and at remission phase (day 15) from 1 patient with plasma cell leukemia, 2) CAR-CD19 T cells collected at day 7 from 11 lymphoma patients treated with Axi-cel and CAR-CD19

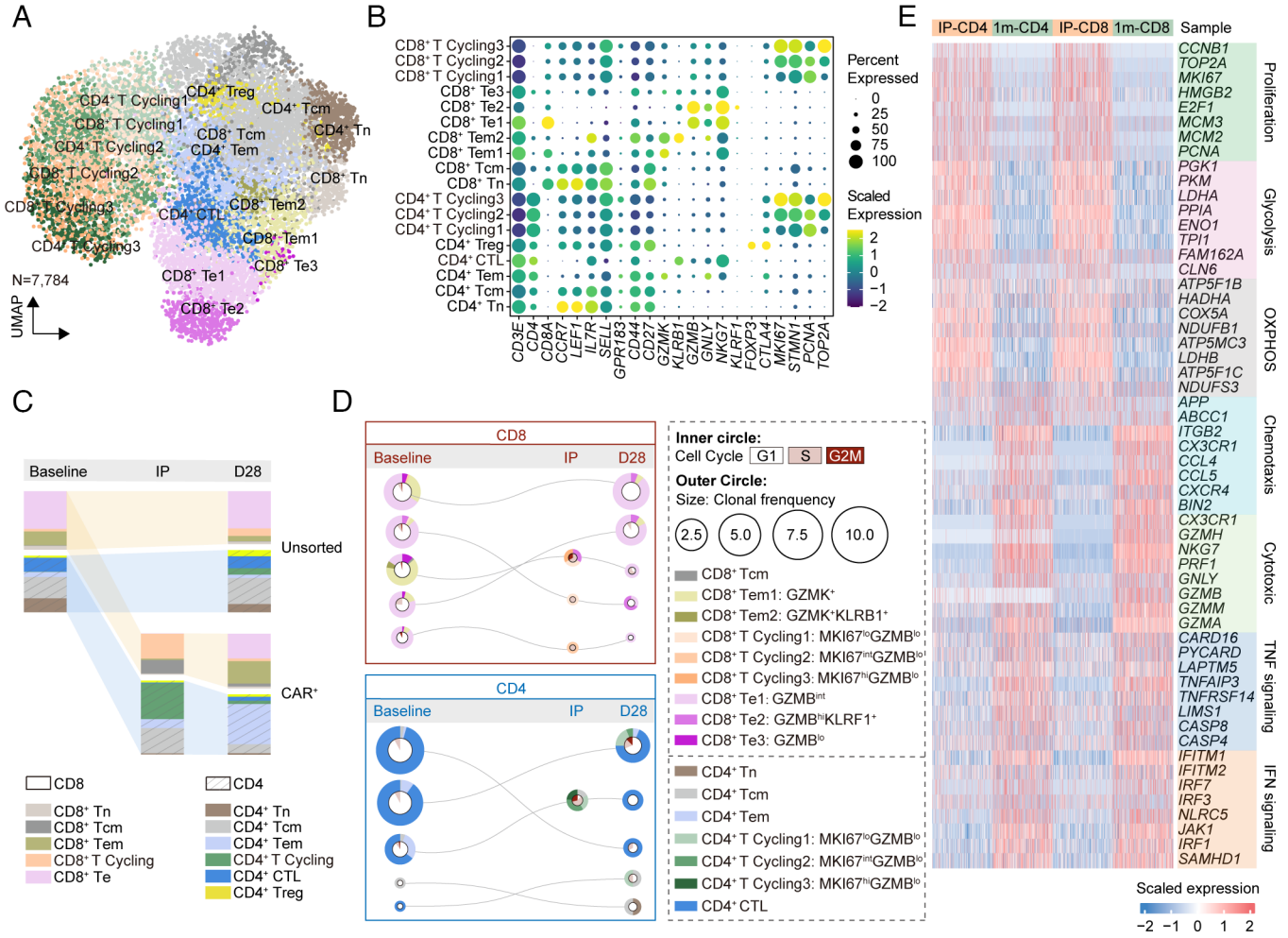

Fig. 5. Transcriptional signature and clone tracking of CAR-T cells in IMNM. (*A*) UMAP plot of CAR-T cells in IPs and at 1 mo post-infusion and endogenous T cells at baseline and at 1 mo post-infusion. (*B*) Dot plot showing cell clusters denoted by gene expression of known markers. (*C*) Depiction of T cell subset frequencies at each timepoint. Bar widths are proportional to the fraction of cells being classified as a particular subset. (*D*) The top five most prevalent TCR clones identified at 1 mo post-treatment and the corresponding clones in IPs or at baseline are shown for CD8$^+$ and CD4$^+$ CAR-T subsets. For each, circles show the clone belongs at each timepoint, with sizes corresponding to the clone frequency in its sample. Pie charts of the inner circle showing the distribution of cells in each phase of the cell cycle. Pie charts of the outer circle showing the distribution of cell types in each subset. (*E*) Heatmap showing the expression of differentially expressed genes of indicated signatures shown by cells from different samples.

T cells collected at day 7 from another 11 lymphoma patients treated with Tisa-cel, 3) CAR-CD19 T cells collected at early phase (~day 7) and at late phase (~day 28) from 3 NHL patients, 4) CAR-CD19 T cells collected at early phase (~day 7), at late phase (~day 28), and at very late phase (~day 90) separately from two CLL patients and two NHL patients. The cells from different datasets were integrated and clustered as they were evenly interspersed across the UMAP plots and could be roughly annotated as four distinct clusters (Fig. 6*A* and *SI Appendix*, Fig. S3). Correlation analysis using the transcriptomics profiles of each dataset revealed a profound overlap between CD8$^+$ CAR-T cells collected at 1 mo from IMNM patient and CD8$^+$ CAR-BCMA T cells in remission phase from a PCL patient (Fig. 6*B*), possibly due to their shared targets and similar stages. Furthermore, the

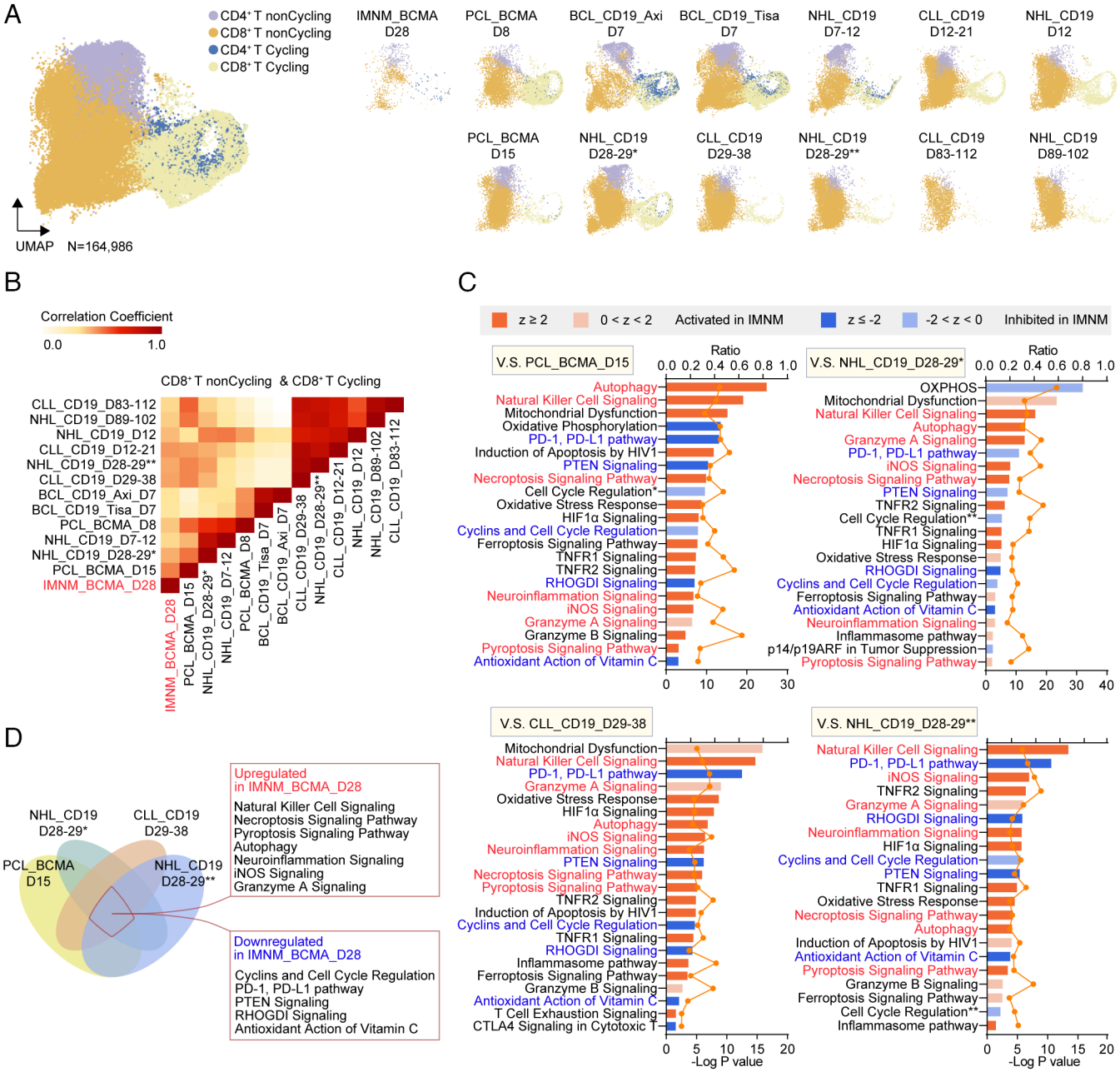

Fig. 6. Distinct signatures of CAR-T cells from patients with IMNM. (*A*) UMAP plots showing the integrating CAR-T cells in vivo originated from patients with IMNM, leukemia, and lymphoma colored by subclusters. Single-cell transcriptomics in four recently published external datasets (GSE151310, GSE197268, GSE166352, and GSE125881), including 1) CAR-BCMA T cells collected at peak phase (day 8) and at remission phase (day 15) from one patient with plasma cell leukemia, 2) CAR-CD19 T cells collected at day 7 from 11 lymphoma patients treated with Axi-cel and CAR-CD19 T cells collected at day 7 from another 11 lymphoma patients treated with Tisa-cel, 3) CAR-CD19 T cells collected at early phase (~day 7) and at late phase (~day 28) from three NHL patients, 4) CAR-CD19 T cells collected at early phase (~day 7), at late phase (~day 28), and at very late phase (~day 90) separately from two CLL patients and two NHL patients, along with our dataset including CAR-T cells collected at 1 mo from the patient with IMNM, were used for signature validation. (IMNM: immune-mediated necrotizing myopathy; PCL: plasma cell leukemia; BCL: B cell lymphoma; NHL: non-Hodgkin lymphoma; CLL: chronic lymphocytic leukemia). (*B*) Heatmap showing the correlations between CD8$^+$ CAR-T cells of integrated conditions. (*C*) Ingenuity pathway analysis comparing CD8$^+$ CAR-T cells collected at 1 mo from IMNM patients with CD8$^+$ CAR-T cells collected at late/remission phase from patients with leukemia and lymphoma. z score reflects the predicted activation level ($z \geq 2$ or $z \leq -2$ can be considered significant). The yellow curve denotes the ratio between the number of the differentially expressed genes (DEGs) and the total number of genes in each of these pathways. Cell Cycle Regulation*, Cell Cycle: G1/S Checkpoint Regulation; Cell Cycle Regulation**, Cell Cycle: G2/M DNA Damage Checkpoint Regulation. (*D*) Venn diagram showing overlapping upregulated and downregulated pathways in CD8$^+$ CAR-T cells collected at 1 mo from IMNM patients when compared with CD8$^+$ CAR-T cells collected at late/remission phase from patients with leukemia and lymphoma.

IMNM CD8$^+$ CAR-T cells were more similar to CAR-T cells from late-stage disease patients with hematological malignancies, rather than early or very late-stage disease patients (Fig. 6*B*), suggesting that these cells were likely to function at a remission/stable phase. However, the CAR-T cells originated from this IMNM patient declined within 2 mo (Fig. 1*C*), not as persistent as CAR-T cells from malignancy patients. Thus, we next conducted Ingenuity Pathway Analysis (IPA) using differentially expressed genes to figure out the possible pathway or mechanism that may contribute to their diminished persistence. Compared to CD8$^+$ CAR-T cells at early/peak phase, IMNM CD8$^+$ CAR-T cells at 1 mo exhibited suppression of OXPHOS, cell cycle, and cancer-related pathway (PD-1, PD-L1 pathway), as well as activated mitochondrial dysfunction, cell death, and neuroinflammation, in accordance with the differences between peak and remission phases (*SI Appendix*, Fig. S4 *A* and *B*). Additionally, compared to late/remission phase CD8$^+$ CAR-T cells, cell death and neuroinflammation were up-regulated while cell cycle pathway remains down-regulated in IMNM CD8$^+$ CAR-T cells at 1 mo (Fig. 6 *C* and *D*), which might be the reason for their decline. Of note, activation of NK cell signaling was also observed (Fig. 6 *C* and *D*), which might lead to T cell exhaustion (11). Collectively, enhanced cell exhaustion/dysfunction, up-regulated cell death, neuroinflammation characterized immune microenvironment, inhibited expansion capacity may be the causes of poor persistence of CAR-T cells in IMNM patients, except for the limited antigen exposure of autoimmune diseases. Conversely, the results were nearly opposite when compared to very late-stage CD8$^+$ CAR-T cells (*SI Appendix*, Fig. S4 *C* and *D*), suggestive of the relatively higher proliferation and effector status of IMNM CD8$^+$ CAR-T cells at 1 mo. Notably, the profound neuroinflammation-related signature was still observed in IMNM CD8$^+$ CAR-T cells, highlighting their unique characteristics derived from IMNM patients.

Discussion

Immune-mediated necrotizing myopathy (IMNM) is an autoimmune disorder characterized by progressive proximal weakness with few extra-muscular manifestations (1). Anti-SRP myopathy is one of the most disabling and refractory subsets of IMNM, often requiring intense, combined, long-term immunosuppressive therapy (2–4). Unfortunately, despite receiving multiple treatments, the disease continues to relapse, as seen in our patient. Our case showed that anti-BCMA CAR-T cell therapy was well-tolerated and brought sustained clinical remission, offering an option for these refractory patients. Of note, the titers of anti-SRP antibody correlate positively with serum CK levels and clinical manifestations (3). The reconstitution of B cell subsets and long-term reduction in autoantibodies we observed in this case might underpin the clinical efficacy.

There is a growing interest in the potential use of CAR-T therapy in treating autoimmune diseases, which was initially developed as a revolutionary treatment for advanced leukemia and lymphoma (12). CAR-T cells targeting CD19 were reported to lead to depletion of CD19-expressing B cells, cessation of autoantibody production, and improvement of clinical symptoms in cases of refractory systemic lupus erythematosus (13, 14) and refractory antisynthetase syndrome (15, 16). Recently, RNA-based anti-BCMA CAR-T cell therapy has shown remarkable therapeutic efficacy in treating 12 patients with refractory myasthenia gravis (17). Similar to our previously published cohort studies involving 12 patients with refractory neuromyelitis optica spectrum disorders (NMOSD) (7) and this highly refractory anti-SRP myopathy patient, CAR-T cells targeting BCMA or CD19 demonstrate significant advantages in treating relapsed/refractory autoimmune diseases, including terrific depletion efficacy, decreased autoantibody titers, and sustained clinical remission during a relatively long follow-up periods. Additionally, considering the restoration of antibody-producing cells with distinct clone types as well as sustained undetected autoantibodies after CAR-T therapy, renewed vaccination might be needed, though more evidence is warranted.

Despite the fact that autoantibodies and B cell repertoire are generally considered hallmarks of autoimmune disorders, recent accumulating evidence suggests that autoimmune T cell lineage and activated immune microenvironment could further contribute to the pathogenesis (18–20) and targeted manipulation of autoimmune T cells might lead to new therapeutic strategies for autoimmune diseases (21). Approximately 25% of IMNM patients exhibit lymphocyte densities, including CD8$^+$ T cells, in the muscle lesions (22) and this raises the possibility of T cell mediated myotoxicity, yet has not been directly observed (3). Thus, we conducted longitudinal scRNA-seq, paired TCR-seq, and paired BCR-seq analysis to evaluate immune alterations following CAR-T therapy. Intriguingly, pathways related to immune response and inflammatory response were down-regulated post-infusion in different cell types, including CD4$^+$ T cells, CD8$^+$ T cells, NK cells, myeloid cells, and restored B cells. Of note, we observed an early-period replacement of higher cytotoxic/inflammatory CD8$^+$ Te-1 cells in expanded T cell lineage by higher chemotaxis and survival CD8$^+$ Te-3 cells, which might aid to eliminate pathogenic cells (23). Moreover, expanded CD8$^+$ Te-3 cells still remained at a certain proportion at the late period of follow-up, accompanied by restoration of CD8$^+$ Te-1 cells with relatively normalized characteristics. These data suggested that CAR-T therapy might contribute to the normalization of T cell-related hyperactivation immune microenvironment in autoimmune disorders indirectly by eliminating autoantibody producing cells.

A major challenge in CAR-T cell therapy for autoimmune diseases is the limited persistence of infused cells, which is observed both in murine models and in clinical trials (5). CAR-T cells treating autoimmune diseases typically become undetectable within 2 mo or even less (7, 13–16), while CAR-T cells treating hematological malignancies can persist for years or even decades (12, 24), which may due to limited antigen exposure, features of pre-manufactured T cells and immune microenvironment post-infusion. To figure out the possible underlined mechanism, we integrated our CAR-T cells in the IMNM patient with CAR-T cells in malignancies patients from published single-cell datasets (25–28). Unlike CAR-T cells at peak phase for proliferation and taking effect or CAR-T cells at very late phase for perhaps exhaustion or withering, IMNM CD8$^+$ CAR-T cells collected at 1 mo tended to function at a remission/stable stage similar to CAR-T cells in malignancies at similar timepoint but presented a more NK-like phenotype with enhanced tendency of cell death and neuroinflammation and inhibited proliferating ability. Notably, neuroinflammation-related signature was observed up-regulated in IMNM CD8$^+$ CAR-T cells when compared with CAR-T cells in malignancies patients at any stage, suggestive of the distinct characteristics of CD8$^+$ CAR-T cells in vivo originated from the IMNM patient.

The current reports on CAR-T therapy in autoimmune diseases show promise in terms of feasibility and potential efficacy, but larger studies with long-term follow-up are needed. Further research, including humanized animal models, is essential to investigate how to enhance the efficacy and persistence of CAR-T cells in treating autoimmune diseases.

Data, Materials, and Software Availability. Raw sequencing data have been deposited in the Genome Sequence Archive in National Genomics Data Center, China National Center for Bioinformation/Beijing Institute of Genomics, Chinese Academy of Sciences (GSA-Human: HRA004636) that will be publicly accessible at https://ngdc.cncb.ac.cn/gsa-human (29).

ACKNOWLEDGMENTS. Our deepest gratitude goes first to Prof. Jian-Feng Zhou, one of our sincere colleagues who died from a heart attack early 2022. We appreciate him for his illuminating instruction and dedication to the project. We also thank Dr. Ying Xiong and Dr. Shuo-Qi Zhang (Department of Radiology, Tongji Hospital) for providing assistance on MRI. We appreciate Jiangsu Simcere Diagnostics Co., Ltd., China, for the technical support of the transcriptional analysis. Ministry of Science and Technology China Brain Initiative Grant STI2030-Major Projects 2022ZD0204700 (Wei Wang). National Natural Science Foundation of China Grants 82071380 (D.-S.T.). National Natural Science Foundation of China Grant 82271341 (C.Q.). Knowledge Innovation Program of Wuhan Shuguang Project 2022020801020454 (C.Q.).

Author affiliations: [a]Department of Neurology, Tongji Hospital, Tongji Medical College, Huazhong University of Science and Technology, Wuhan 430030, China; [b]Hubei Key Laboratory of Neural Injury and Functional Reconstruction, Huazhong University of Science and Technology, Wuhan 430030, China; [c]Nanjing IASO Biotherapeutics Ltd., Nanjing 210000, China; and [d]Department of Hematology, Tongji Hospital, Tongji Medical College, Huazhong University of Science and Technology, Wuhan 430030, China

1. Y. Allenbach, A. L. Mammen, O. Benveniste, W. Stenzel, Immune-mediated necrotizing myopathies working G 224th ENMC International Workshop: Clinico-sero-pathological classification of immune-mediated necrotizing myopathies Zandvoort, The Netherlands, 14–16 October 2016. *Neuromuscul. Disord.* **28**, 87–99 (2018).
2. C. Anquetil, O. Boyer, N. Wesner, O. Benveniste, Y. Allenbach, Myositis-specific autoantibodies, a cornerstone in immune-mediated necrotizing myopathy. *Autoimmun. Rev.* **18**, 223–230 (2019).
3. J. A. Day, V. Limaye, Immune-mediated necrotising myopathy: A critical review of current concepts. *Semin. Arthritis. Rheum.* **49**, 420–429 (2019).
4. A. Selva-O'Callaghan *et al.*, Classification and management of adult inflammatory myopathies. *Lancet Neurol.* **17**, 816–828 (2018).
5. D. J. Baker, C. H. June, CAR T therapy extends its reach to autoimmune diseases. *Cell* **185**, 4471–4473 (2022).
6. D. Wang *et al.*, A phase 1 study of a novel fully human BCMA-targeting CAR (CT103A) in patients with relapsed/refractory multiple myeloma. *Blood* **137**, 2890–2901 (2021).
7. C. Qin *et al.*, Anti-BCMA CAR T-cell therapy CT103A in relapsed or refractory AQP4-IgG seropositive neuromyelitis optica spectrum disorders: Phase 1 trial interim results. *Signal Transduct. Target. Ther.* **8**, 5 (2023).
8. L. Amini *et al.*, Preparing for CAR T cell therapy: Patient selection, bridging therapies and lymphodepletion. *Nat. Rev. Clin. Oncol.* **19**, 342–355 (2022).
9. N. Saligrama *et al.*, Opposing T cell responses in experimental autoimmune encephalomyelitis. *Nature* **572**, 481–487 (2019).
10. J. Li *et al.*, KIR(+)CD8(+) T cells suppress pathogenic T cells and are active in autoimmune diseases and COVID-19. *Science* **376**, eabi9591 (2022).
11. C. R. Good *et al.*, An NK-like CAR T cell transition in CAR T cell dysfunction. *Cell* **184**, 6081–6100. e6026 (2021).
12. S. J. Schuster *et al.*, Chimeric antigen receptor T cells in refractory B-cell lymphomas. *N. Engl. J. Med.* **377**, 2545–2554 (2017).
13. D. Mougiakakos *et al.*, CD19-targeted CAR T cells in refractory systemic lupus erythematosus. *N. Engl. J. Med.* **385**, 567–569 (2021).
14. A. Mackensen *et al.*, Anti-CD19 CAR T cell therapy for refractory systemic lupus erythematosus. *Nat. Med.* **28**, 2124–2132 (2022).
15. F. Muller *et al.*, CD19-targeted CAR T cells in refractory antisynthetase syndrome. *Lancet* **401**, 815–818 (2023).
16. A. C. Pecher *et al.*, CD19-targeting CAR T cells for myositis and interstitial lung disease associated with antisynthetase syndrome. *JAMA* **329**, 2154–2162 (2023).
17. V. Granit *et al.*, Safety and clinical activity of autologous RNA chimeric antigen receptor T-cell therapy in myasthenia gravis (MG-001): A prospective, multicentre, open-label, non-randomised phase 1b/2a study. *Lancet Neurol.* **22**, 578–590 (2023).
18. M. C. Dalakas, R. Hohlfeld, Polymyositis and dermatomyositis. *Lancet* **362**, 971–982 (2003).
19. L. Gallay, C. Gayed, B. Hervier, Antisynthetase syndrome pathogenesis: Knowledge and uncertainties. *Curr. Opin. Rheumatol.* **30**, 664–673 (2018).
20. F. Rosetti, I. K. Madera-Salcedo, N. Rodriguez-Rodriguez, J. C. Crispin, Regulation of activated T cell survival in rheumatic autoimmune diseases. *Nat. Rev. Rheumatol.* **18**, 232–244 (2022).
21. E. F. McKinney, J. C. Lee, D. R. Jayne, P. A. Lyons, K. G. Smith, T-cell exhaustion, co-stimulation and clinical outcome in autoimmunity and infection. *Nature* **523**, 612–616 (2015).
22. Y. Allenbach *et al.*, Necrosis in anti-SRP(+) and anti-HMGCR(+)myopathies: Role of autoantibodies and complement. *Neurology* **90**, e507–e517 (2018).
23. Z. S. Chheda, R. K. Sharma, V. R. Jala, A. D. Luster, B. Haribabu, Chemoattractant receptors BLT1 and CXCR3 regulate antitumor immunity by facilitating CD8+ T cell migration into tumors *J. Immunol.* **197**, 2016–2026 (2016).
24. J. J. Melenhorst *et al.*, Decade-long leukaemia remissions with persistence of CD4(+) CAR T cells. *Nature* **602**, 503–509 (2022).
25. X. Li *et al.*, Single-cell transcriptomic analysis reveals BCMA CAR-T Cell dynamics in a patient with refractory primary plasma cell leukemia. *Mol. Ther.* **29**, 645–657 (2021).
26. N. J. Haradhvala *et al.*, Distinct cellular dynamics associated with response to CAR-T therapy for refractory B cell lymphoma. *Nat. Med.* **28**, 1848–1859 (2022).
27. J. Zhang *et al.*, Non-viral, specifically targeted CAR-T cells achieve high safety and efficacy in B-NHL. *Nature* **609**, 369–374 (2022).
28. A. Sheih *et al.*, Clonal kinetics and single-cell transcriptional profiling of CAR-T cells in patients undergoing CD19 CAR-T immunotherapy. *Nat. Commun.* **11**, 219 (2020).
29. C. Qin *et al.*, Single-cell RNA-Seq reveals transcriptional characteristics in human autoimmune neurologic diseases and cellular dynamics after BCMA-targeting CAR-T therapy. Genome Sequence Archive for Human. https://ngdc.cncb.ac.cn/search/?dbId=hra&q=HRA004636. Deposited 22 May 2023.